

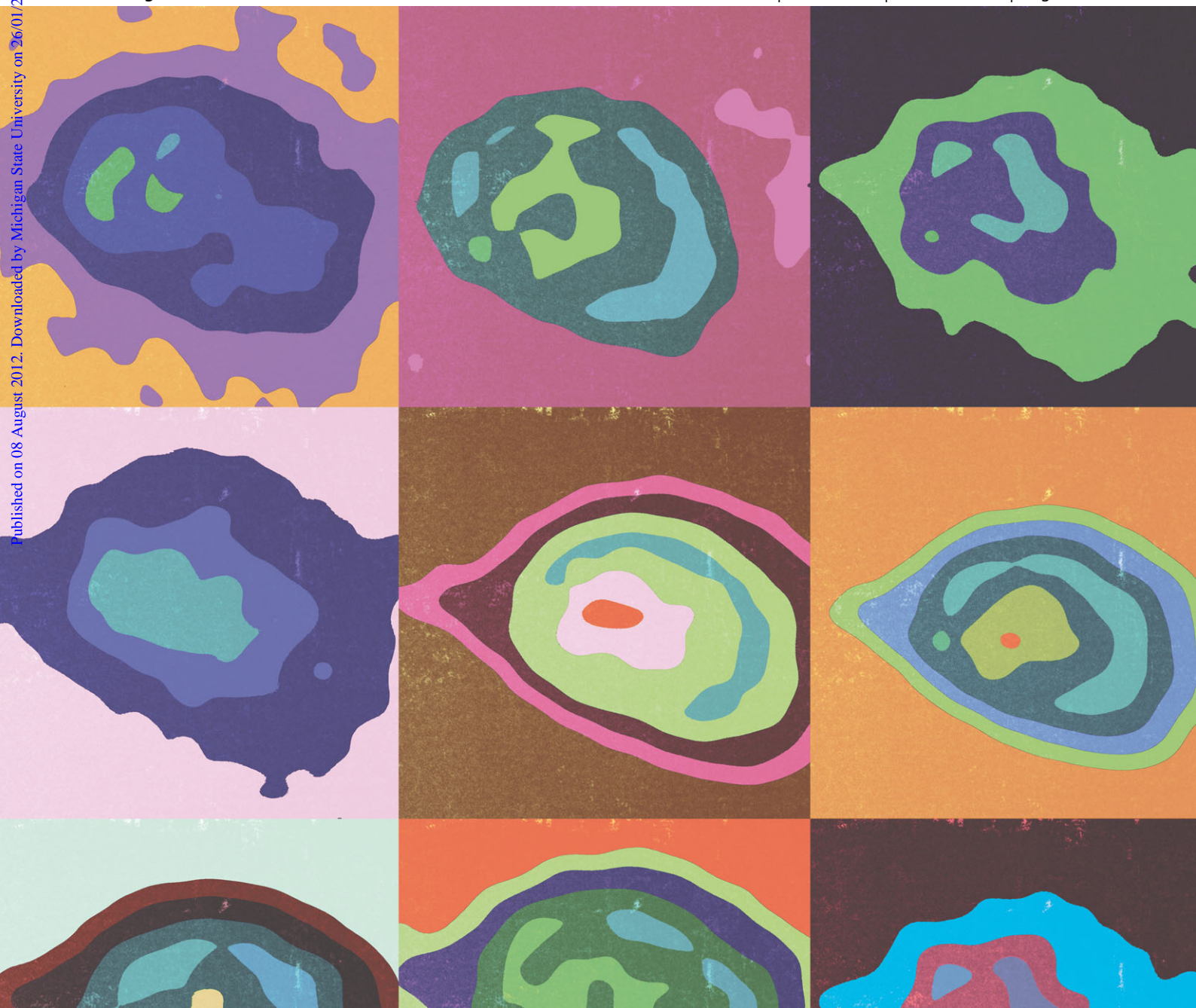
Metallomics

Integrated biometal science

www.rsc.org/metallomics

Volume 4 | Number 10 | October 2012 | Pages 1007–1126

Published on 08 August 2012. Downloaded by Michigan State University on 26/01/2016 20:17:48.



ISSN 1756-5901

PAPER

Hugh H. Harris *et al.*
Distinct cellular fates for KP1019
and NAMI-A determined by X-ray
fluorescence imaging of single cells

Indexed in
MEDLINE!



1756-5901(2012)4:10;1-S

RSC Publishing

Distinct cellular fates for KP1019 and NAMI-A determined by X-ray fluorescence imaging of single cells[†]

Jade B. Aitken,^{a,b,c} Sumy Antony,^{d,e} Claire M. Weekley,^e Barry Lai,^f Leone Spiccia^d and Hugh H. Harris^{*e}

Received 23rd April 2012, Accepted 6th August 2012

DOI: 10.1039/c2mt20072d

Small molecule ruthenium complexes show great promise as anticancer pharmaceuticals, but further rational development of these as drugs is stymied by an incomplete understanding of the mechanisms that give rise to markedly different biological behaviour for structurally similar species. X-ray fluorescence imaging at two incident energies was used to reveal the intracellular distribution of Ru in single human cells treated with KP1019, showing Ru localised in both cytosol and in the nuclear region. In addition the imaging showed that treatment with KP1019 modulated Fe distribution to resemble the Ru distribution, without affecting cellular Fe content. In stark contrast, Ru could not be visualised in cells treated with NAMI-A, indicating that it was not internalised and supporting the proposition that its activity is exerted through a membrane-binding mechanism.

Introduction

Several approaches aimed at improving metal-based anti-cancer agents are currently demonstrating potential in pre-clinical and clinical settings.^{1–3} Despite its continued clinical application, the archetypal cisplatin displays high toxicity, a narrow spectrum of activity and, commonly, resistance (either acquired or intrinsic) from various cancers.^{4,5} Ruthenium complexes^{6–8} in various guises have shown anticancer activity

combined with partial or complete loss of one or more of the problems associated with the use of cisplatin. Two Ru(II) anti-cancer drugs have successfully completed Phase I clinical trials, *trans*-[Ru^{III}(dmso)(Im)Cl₄][ImH] (NAMI-A, Im = imidazole, dmso = dimethylsulfoxide) and *trans*-[Ru^{III}(Ind)₂Cl₄][IndH] (KP1019, Ind = indazole).⁹ Despite their apparent structural similarity they exhibit markedly different anticancer activities: NAMI-A has little effect on primary tumour sites but inhibits metastasis formation¹⁰ and reduces metastases' weight;¹¹ KP1019, in contrast, shows activity against a wide range of primary tumours by inducing apoptosis.^{12,13} Importantly, both NAMI-A¹⁴ and KP1019⁹ showed limited side effects with only mild toxicity in their initial clinical trials. KP1019 failed to progress to phase II clinical trials due to low solubility preventing an escalation of the dosage above 600 mg per patient, and subsequent determination of a maximum tolerated dose.¹⁵ It is apparent that an understanding of the *in vivo* chemistry of the two complexes that leads to an explanation for their distinct biological behaviour could inform the development of future, related, ruthenium-based anticancer agents.

Two processes, transport into cells by transferrin receptors and activation by reduction, have been suggested to explain the increased selectivity of KP1019 resulting in a higher anticancer activity.^{16,17} The rapid division of cancerous cells introduces a higher requirement for iron and therefore transferrin receptors are overexpressed, making them good targets for anticancer agents and providing justification for pursuing ruthenium anticancer agents.^{4,7,18} It has been proposed that transferrin plays a significant role in the transportation of KP1019, or its metabolites, into the cell.^{12,19} Secondly, tumour tissue

^a School of Chemistry, The University of Sydney, New South Wales, 2006, Australia

^b Australian Synchrotron, Clayton, Victoria, 3168, Australia

^c Institute of Materials Structure Science, KEK, Tsukuba, Ibaraki 305-0801, Japan

^d School of Chemistry, Monash University, VIC 3800, Australia

^e School of Chemistry and Physics, The University of Adelaide, SA 5005, Australia. E-mail: hugh.harris@adelaide.edu.au; Tel: +61 8 8303 5060

^f X-ray Science Division, Argonne National Laboratory, Argonne IL 60439, USA

[†] Electronic supplementary information (ESI) available: Table S1: Elemental area densities within cultured SH-SY5Y cells (control) and cells treated with either NAMI-A or KP1019 for 4 h. Fig. S1: Splitting pattern for NAMI-A. Fig. S2: Accurate mass spectrum of NAMI-A. Fig. S3: Electrospray mass spectrum for NAMI-A; Cone 15 V; Solvent – DMF/CAN. Fig. S4: Splitting pattern for KP1019. Fig. S5: Accurate mass spectrum of KP1019. Fig. S6: Electrospray mass spectrum for KP1019. Fig. S7–S9: XRF elemental distribution maps of SH-SY5Y cells treated with KP1019. Fig. S10–S14: XRF elemental distribution maps of untreated SH-SY5Y cells. Fig. S15–S17: XRF elemental distribution maps of SH-SY5Y cells treated with NAMI-A. Fig. S18–S20 Representative integrated X-ray fluorescence spectra for control and cells treated with KP1019 or NAMI-A. Table S2: Calculated Ru K α signal and error magnitude for NAMI-A treated cells. See DOI: 10.1039/c2mt20072d

typically forms a reducing environment as a result of a poor oxygen supply due to insufficient vasculature.¹² An activation by reduction theory suggests that the relatively inactive Ru(III) complexes are pro-drugs that are reduced intracellularly to generate more active species.^{18,20} It is hypothesised that after entry into the cell attached to transferrin, Ru(III) is converted to Ru(II) in a similar fashion to iron, but it is unclear what is responsible for the reduction.¹² Within the cell the most common reductant is glutathione, however, this has been found to inhibit KP1019 Ru–DNA interactions through the formation of Ru(II)–glutathione complexes.¹² Meanwhile, ascorbate does not effectively reduce ruthenium in KP1019 under physiological conditions³ and no evidence exists *in vivo* to demonstrate that reduction either occurs or is critical to activity of the drug.¹²

The mode of action of NAMI-A is likely to be different to that of both cisplatin and KP1019 due to the low cytotoxicity of NAMI-A and its targeting of metastatic cancer. NAMI-A hydrolyses *in vivo* forming a number of potentially active species²¹ but is not cytotoxic *in vitro*.⁷ Bergamo *et al.* have suggested that NAMI-A is not internalised in cells, as it has a slow uptake compared to clearance from the blood stream,^{22,23} and therefore must act at an extracellular level.^{13,24,25} DNA was excluded as a primary target for NAMI-A due to observed effects such as anti-angiogenic activity^{26,27} and significant interaction of NAMI-A with integrins was demonstrated.²⁸ NAMI-A affected the interactions of A549 cultured cells with collagen, decreasing cell adhesion and mobility.^{13,29} In contrast to KP1019, the binding of NAMI-A to serum albumin or serum transferrin results in a significant loss of biological activity.^{2,27}

We, and others, have demonstrated the utility of X-ray fluorescence (XRF) microprobe imaging of single cultured cells, treated with metal and metalloid species, as a method to determine intracellular targets for those compounds as a function of treatment time and other experimental conditions.^{26,30–33} The technique is amenable to the similar study of the ruthenium based anticancer drugs, however the inconvenient energies of the L emission lines for ruthenium, which are coincident with abundant endogenous elements such as potassium and calcium, combined with the high K-edge energy, which provides numerous instrumental challenges, have so far precluded useful results. Herein, we describe the first use of XRF imaging to reveal the cellular distribution of ruthenium in cells treated with KP1019 or NAMI-A. This represents the first study to investigate the cellular distribution of these species that does not involve a cell lysis step, which has been shown to cause a modulation of cellular distribution for another exogenous metal.³⁴

Experimental

Instrumentation

Microanalyses (C, H, and N) were performed by Campbell Microanalytical Service, Otago, New Zealand. *Low-resolution electrospray mass spectra* were obtained with a Micromass Platform II Quadrupole Mass Spectrometer fitted with an electrospray source. The capillary voltage was at 3.5 eV,

and the cone voltage was at 15 V. *Accurate high-resolution mass spectra* were obtained with a Bruker BioApex II 47e FT-ICR MS instrument fitted with an Analytical Electrospray Source. Samples were introduced by a syringe pump at a rate of 1 $\mu\text{L min}^{-1}$ and the capillary voltage was 120 V. *UV-vis-NIR spectra* were recorded on 0.1–2 mM solutions in quartz cuvettes using Varian Cary spectrophotometer.

Preparation of KP1019 and NAMI-A

trans-[Ru^{III}(dmso)(Im)Cl₄][ImH] (NAMI-A, Im = imidazole, dmso = dimethyl sulfoxide) and *trans*-[Ru^{III}(Ind)₂Cl₄][IndH] \cdot H₂O (KP1019, Ind = indazole) were prepared according to literature methods^{20,35–37} and their identity was confirmed using elemental analysis, electrospray ionisation mass spectrometry and UV-Vis spectroscopy.

Analysis

Calc. for NAMI-A C₈H₁₅N₄Cl₄ORuS: C 20.97, H 3.30, N 12.23%, *Found* C 21.31, H 3.24, N 12.33%. *Calc.* for KP1019 C₂₁H₁₉N₆Cl₄Ru \cdot H₂O: C 40.92, H 3.43, N 13.64%, *Found* C 41.02, H 3.28, N 13.73%. ESI-MS (DMF/ACN, –ve ion): *m/z* NAMI-A: 389.7 (Fig. S1–S3, ESI \ddagger), *m/z* KP109: 479.7, (Fig. S4–S6, ESI \ddagger). UV-Vis (MeOH – data not shown): λ_{max} (nm) ϵ_{max} (M^{–1} cm^{–1}): NAMI-A: 397 (3790); KP109: 370 (3510).

Cell culture

SH-SY5Y human neuroblastoma cells, originally purchased from the American Tissue Culture Collection, were a gift from Paul Witting (The University of Sydney). Cells were cultured as monolayers in Dulbecco's modified Eagle's medium (DMEM-F12) supplemented with fetal bovine serum (10%, v/v), L-glutamine (2 mM), an antibiotic–antimycotic mixture (100 mg mL^{–1} penicillin and 100 units per mL streptomycin), and nonessential amino acids (100 units per mL) at 310 K in a 5% CO₂-humidified incubator and were subcultured every 3–7 days.

Preparation of whole cells for analysis

SHSY-5Y human neuroblastoma cells were grown directly on 500 nm thick silicon nitride windows (Silson Pty Ltd) as described previously.³⁸ Cells were treated for 4 h with either KP1019 or NAMI-A (200 μM final concentration in complete media, prepared immediately from 50 mM DMF stock solutions) or DMF alone in complete media (control). Following treatment the cells were fixed in paraformaldehyde and then dipped (5 times) in cold methanol. Normal cell morphology was retained throughout the treatment and fixation procedures as evidenced in the optical micrographs (shown below).

X-ray fluorescence mapping of the cells at 0.5 μm resolution was performed at the Advanced Photon Source (APS) beamline 2-ID-D, Chicago (USA) with modifications to the protocol described previously.^{33,38–40} All measurements were conducted using either a monochromatic 10.0 or 22.5 keV X-ray beam focused using a dual zone plate and order sorting aperture device. P to Zn elemental distribution maps were collected at 10.0 keV and the Ru data at 22.5 keV. The fluorescence signal was detected for 1 s per spatial point at 90° to the incident beam

using a single-element solid-state UltraLEGe detector (Canberra). Quantitation (elemental area densities in micrograms per square centimeter, $\mu\text{g cm}^{-2}$) was performed using MAPS software²² by fitting the full fluorescence spectrum at every spatial point to modified Gaussians and comparing with corresponding measurements on the thin-film standards NBS-1832 and NBS-1833 from the National Bureau of Standards (Gaithersburg, MD, USA). The statistical significance of changes in the elemental content of treated cells compared to controls (Table S1, ESI†) was assessed using a two-tailed Mann–Whitney test at the 99% confidence level.

Results and discussion

XRF elemental mapping of single SH-SY5Y cells treated with 200 μM KP1019 for 4 h (Fig. 1 and Fig. S7–S9, ESI†) revealed a significant increase of intracellular ruthenium compared to the vehicle-alone treated control cells (Fig. 2 and Fig. S10–S14, ESI†), where ruthenium was not detected (Table S1, ESI†). Ruthenium content was found to significantly increase in both whole treated cells and their nuclear region (as defined by regions of colocalisation of P and Zn, Table S1, ESI†). There was a significant increase in the elemental densities of Cu in both the whole cells and nuclear region of cells treated with KP1019, compared to the controls, (Table S1, ESI†).

The ruthenium content in the nuclear region was determined to be $\sim 50\%$ of the total cellular content after 4 hours of treatment with KP1019. Several previous studies have demonstrated uptake of KP1019 by cultured cells in a range of cell

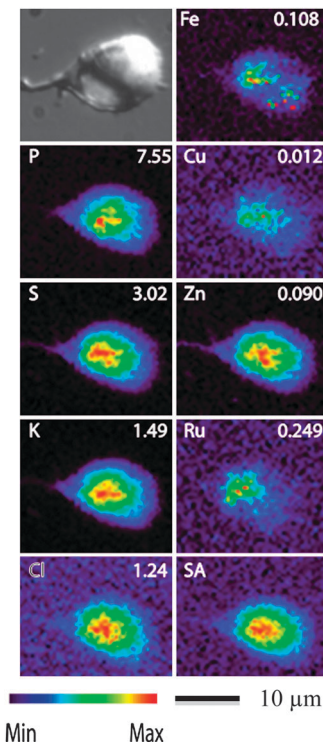


Fig. 1 Optical micrograph (top left), scattered X-ray (SA) and XRF elemental distribution maps of P, S, K, Cl, Fe, Cu, Zn, and Ru of a SH-SY5Y cell treated with 200 μM KP1019 for 4 h. Maximal area densities are given in $\mu\text{g cm}^{-2}$ for each element.

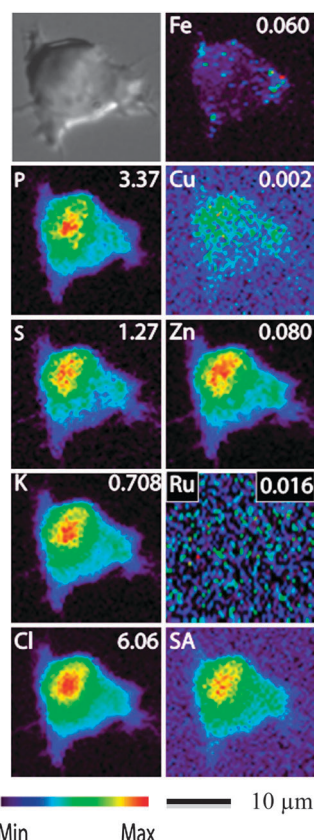


Fig. 2 Optical micrograph (top left), scattered X-ray (SA) and XRF elemental distribution maps of P, S, K, Cl, Fe, Cu, Zn, and Ru of an untreated SH-SY5Y cell. Maximal area densities are given in $\mu\text{g cm}^{-2}$ for each element.

lines using ICP-MS and determined cellular partitioning across cytoplasmic and nuclear compartments by fractionation methods. The nuclear partitioning results reported ranged from $\sim 20\%$ in A2780 cells² (both cisplatin resistant and sensitive), to $\sim 25\%$ in KB-3-1 cells¹³ and to as high as 55% in SW480 cells.²⁶ This variation may perhaps be ascribed to the different cell lines employed displaying distinct metabolisms of the drug; we note that treatment times and concentrations, as well as exact fractionation methodology, varied between the three reports. Nonetheless, the gross observation was that in all cases ruthenium was detected at significant levels in both the nucleus and in other parts of the cell. Our results are consistent with this observation, however, our figure for nuclear ruthenium content is likely an overestimation. This is an artifact of measuring a three-dimensional object projected into two dimensions, combined with the fact that the nucleus in the cells comprises a considerable portion of the total area. It is hence reasonable that a significant amount of non-nuclear material may over- or underlie the nucleus in the images and be incorrectly included in the nuclear fraction leading to an overestimation.

Fig. 3 illustrates the distribution of Fe compared to Ru (column a), P compared to Ru (column b) and a P elemental distribution map to show the cell area (column c) for the four SH-SY5Y cells (one in each row) treated with 200 μM KP1019 for 4 hours. To increase clarity, only the areas of highest

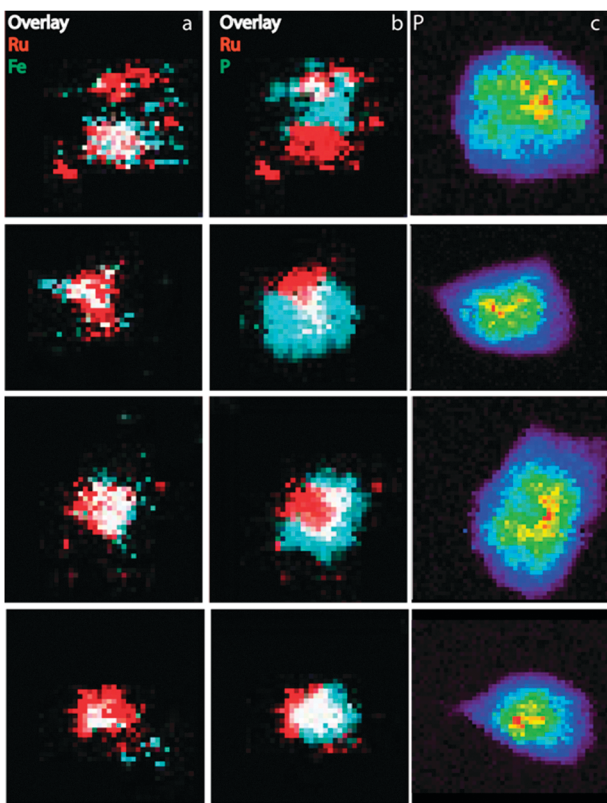


Fig. 3 XRF elemental distribution maps of SH-SY5Y cells treated with 200 μM KP1019 for 4 h showing the colocalisation of (a) Ru(red), Fe(green), overlap (*i.e.* an area where both elements are abundant – white); (b) Ru(red), P(green), overlap (white); (c) the P elemental distribution map.

intensity for each element are shown. Although there was no statistically significant change in the cellular content of iron, Fig. 1 (and Fig. S7–S9, ESI†) demonstrates a change in the intracellular distribution compared to the control cells (Fig. 2 and Fig. S10–S14, ESI†). Iron was found in a punctate distribution throughout the control cells and in the KP1019 treated cells. However, an additional pool of iron was observed in regions of high concentration that were partially colocalised with ruthenium in the treated cells. Consideration of all four cells shown in Fig. 3 suggests that this localisation is proximal to, rather than inside, the nucleus.

The effectiveness of ruthenium pharmaceuticals has been ascribed to three properties: slow ligand exchange kinetics which mimic the time scale for cell division processes; multiple physiologically accessible oxidation states allowing “activation by reduction” (*e.g.*, Ru(III) \rightarrow Ru(II)) enabling transport without compositional change, and; the ability to mimic iron in binding to biological molecules allowing transport to key biological targets.^{20,36} Additional evidence to support the last of these hypotheses includes circular dichroism and electrospray ionisation mass spectrometry studies which showed that some ruthenium was taken up into cells *via* transferrin receptors, but also that this was not the only pathway of entry.²⁶ In addition, a physiologically relevant iron concentration was necessary for the most effective uptake of KP1019, with iron binding to one of the two binding sites of transferrin.²⁶

Although a simplified view of ruthenium drugs as platinum-drug analogs which cause DNA damage has been considered and studied extensively,³⁶ Heffter found that despite ruthenium being present in the nucleus, its cytotoxicity was independent of p53 status and therefore acts in a manner that is unlike DNA-damaging drugs such as cisplatin.¹³ When comparing cisplatin sensitive against resistant cells, Groessl *et al.* determined that there was some damage to DNA as a result of KP1019 uptake into both cell types.² Taken together with the variation in reported cellular partitioning discussed above, these observations suggest that the mechanism, or mechanisms, by which KP1019 exerts its toxicity is yet to be fully established. Our observation that treatment with KP1019 leads to partial colocalisation of ruthenium and iron in the cell is consistent with the idea of adventitious involvement of ruthenium drugs in iron uptake and metabolism, but the observed modulation of iron distribution indicates that perturbation of iron metabolism by ruthenium drugs, and the possibility that toxicity is related to that perturbation, should also be considered in future.

Within KP1019 treated cells we observe two other main sites of ruthenium within the cell: in the cytosol region, but not coincident with the regions of high iron intensity, and; in an area overlapping and adjacent to the regions of high P intensity that are indicative of the nuclear region (Fig. 3b). These findings are consistent with those of Pongratz *et al.* in that there is a requirement of iron bound to transferrin as well as a separate uptake mechanism to achieve delivery of ruthenium to the cytoplasm before its transport to the nucleus.²⁶ At the same time this does not preclude the possibility that the metabolisms of ruthenium and iron may bifurcate at some stage (perhaps after putative release of the metal from a transferrin complex in the acidic environment of endosomes) leading to distinct distributions.

The XRF elemental mapping of single 200 μM NAMI-A-treated SH-SY5Y cells (Fig. 4 and Fig. S15–S17, ESI†) revealed a statistically significant increase in ruthenium compared to the control cells in both the whole cell and the nuclear region (Table S1, ESI†). Despite this, the level of ruthenium in the cells was insufficient to discern its distribution within the cell from the background. This indicates that the level of ruthenium was below the detection limit of the instrument when considered at a single spatial point in the mapping process, but that integration of the signal over larger areas led to a reduction in the detection limit to the point where ruthenium content could be determined. The confidence in detection of ruthenium in the integrated region is supported by comparison of the energy region surrounding ~ 19 keV in the fluorescence spectrum of a single NAMI-A treated cell (Fig. S20, ESI†) where a peak corresponding to ruthenium K α emission is clearly evident, compared to that of an untreated cell where the peak is not evident (Fig. S18, ESI†). This is further supported by the positive net signal calculations showing a positive integration of the Ru K α signal compared to the background along with a calculated average Ru K α signal in excess of five times the magnitude of the average calculated error (Table S2, ESI†).

The NAMI-A-treated cells showed significant increases in the level of Cu both within the total cell and the cell

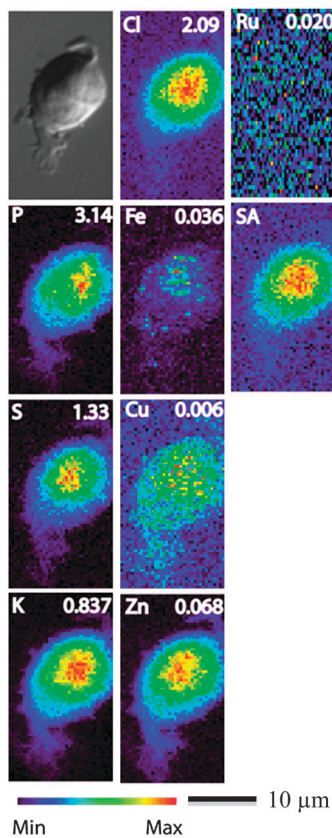


Fig. 4 Optical micrograph (top left), scattered X-ray (SA) and XRF elemental distribution maps of P, S, K, Cl, Fe, Cu, Zn, and Ru of a SH-SY5Y cell treated with 200 μM NAMI-A for 4 h. Maximal area densities are given in $\mu\text{g cm}^{-2}$ for each element.

nucleus (Table S1, ESI†). The absence of significant changes in other elemental content or distribution within the cell (in particular, iron), that were present in cells treated with KP1019, is also indicative that NAMI-A is not entering the cell.

Dyson *et al.*, found NAMI-A primarily in the particulate fraction of cells which includes the plasma membrane,² apparently due to interaction with extracellular or external cell membrane receptor proteins.^{36,41} Frausin *et al.*⁴² determined that the antimetastatic activity of NAMI-A is exerted by inducing conformational changes on extracellular sites of the cell membrane. Our results support those findings that indicate there is no binding of NAMI-A to DNA and that the primary binding site is extracellular, albeit at a very low concentration in these experiments.

Conclusions

The μ -XRF studies clearly show that KP1019 and NAMI-A have different cellular fates, supporting previous studies but utilising a technique that does not involve cell lysis. The observed colocalisation of ruthenium with iron, along with the change in distribution of iron upon treatment with KP1019 provides further evidence that ruthenium enters the cells *via* transferrin receptors, and more generally, that it is involved in, and may disrupt, iron metabolism. Cells treated with KP1019

showed a colocalisation of P with Ru, indicative of uptake of the drug into the nucleus, whereas there was no change in the cellular elemental distribution upon treatment with NAMI-A.

We have shown that synchrotron-based XRF is capable of detecting intracellular ruthenium and can provide valuable insight into the metabolic pathway of ruthenium-based drugs. Unfortunately this capability does not, in this instance, extend to situations where cells do not internalise drugs, such as that which is apparent for NAMI-A. However, when combined with cellular uptake experiments, μ -XRF studies can be considered as a powerful tool, in the context of drug development, to determine the mechanism of action of drugs which are internalised. These studies may be taken as a basis for developmental strategies of the analogues of NAMI-A and KP1019 and their anticancer properties. In future studies, μ -XRF experiments will be undertaken to investigate the intracellular ruthenium distribution in cancer cells treated with various analogues of NAMI-A and KP1019.

Acknowledgements

The authors thank David Benjafield for his generous assistance in figure preparation. This work was funded by the Australian Research Council (DP0985807-QEII to H.H.H, DP0984722 to H.H.H.) We acknowledge travel funding provided by the International Synchrotron Access Program (ISAP) managed by the Australian Synchrotron and funded by the Australian Government. The use of the Advanced Photon Source was supported by the USA Dept of Energy, Office of Science, under contract no. W-31-109-Eng-38.

Notes and references

- U. Jungwirth, C. R. Kowol, B. K. Keppler, C. G. Hartinger, W. Berger and P. Heffeter, *Antioxid. Redox Signaling*, 2011, **15**, 1085–1127.
- M. Groessl, O. Zava and P. J. Dyson, *Metallomics*, 2011, **3**, 591–599.
- A. Levina, A. Mitra and P. A. Lay, *Metallomics*, 2009, **1**, 458–470.
- P. J. Dyson and G. Sava, *Dalton Trans.*, 2006, 1929–1933.
- T. W. Hambley, *Coord. Chem. Rev.*, 1997, **166**, 181–223.
- R. E. Morris, R. E. Aird, P. del Socorro Murdoch, H. Chen, J. Cummings, N. D. Hughes, S. Parsons, A. Parkin, G. Boyd, D. I. Jodrell and P. J. Sadler, *J. Med. Chem.*, 2001, **44**, 3616–3621.
- W. H. Ang and P. J. Dyson, *Eur. J. Inorg. Chem.*, 2006, 4003–4018.
- C. G. Hartinger, A. D. Phillips and A. A. Nazarov, *Curr. Top. Med. Chem.*, 2011, **11**, 2688–2702.
- C. G. Hartinger, S. Zorbas-Seifried, M. A. Jakupcak, B. Kynast, H. Zorbas and B. K. Keppler, *J. Inorg. Biochem.*, 2006, **100**, 891–904.
- M. Cocchietto, S. Zorzet, A. Sorc and G. Sava, *Invest. New Drugs*, 2003, **21**, 55–62.
- G. Sava, S. Zorzet, C. Turrin, F. Vita, M. Soranzo, G. Zabucchi, M. Cocchietto, A. Bergamo, S. DiGiovine, G. Pezzoni, L. Sartor and S. Garbisa, *Clin. Cancer Res.*, 2003, **9**, 1898–1905.
- C. G. Hartinger, M. A. Jakupcak, S. Zorbas-Seifried, M. Groessl, A. Egger, W. Berger, H. Zorbas, P. J. Dyson and B. K. Keppler, *Chem. Biodiversity*, 2008, **5**, 2140–2155.
- P. Heffeter, K. Boeck, B. Atil, M. A. R. Hoda, W. Koerner, C. Bartel, U. Jungwirth, B. K. Keppler, M. Micksche, W. Berger and G. Koellensperger, *JBIC, J. Biol. Inorg. Chem.*, 2010, **15**, 737–748.
- J. M. Rademaker-Lakhai, *Clin. Cancer Res.*, 2004, **10**, 3717–3727.
- A. Bergamo, C. Gaiddon, J. H. M. Schellens, J. H. Beijnen and G. Sava, *J. Inorg. Biochem.*, 2012, **106**, 90–99.
- A. R. Timerbaev, A. V. Rudnev, O. Semenova, C. G. Hartinger and B. K. Keppler, *Anal. Biochem.*, 2005, **341**, 326–333.
- P. Schluga, C. G. Hartinger, A. Egger, E. Reisner, M. Galanski, M. A. Jakupcak and B. K. Keppler, *Dalton Trans.*, 2006, 1796–1802.

- Published on 08 August 2012. Downloaded by Michigan State University on 26/01/2016 20:17:48.
-
- 18 N. Cetinbas, M. I. Webb, J. A. Dubland and C. J. Walsby, *JBIC, J. Biol. Inorg. Chem.*, 2010, **15**, 131–145.
- 19 G. Sava, S. Zorzet, T. Giraldi, G. Mestroni and G. Zassinovich, *Eur. J. Cancer Clin. Oncol.*, 1984, **20**, 841–847.
- 20 E. S. Antonarakis and A. Emadi, *Cancer Chemother. Pharmacol.*, 2010, **66**, 1–9.
- 21 E. Alessio, G. Mestroni, A. Bergamo and G. Sava, *Curr. Top. Med. Chem.*, 2004, **4**, 1525–1535.
- 22 S. Vogt, *J. Phys. IV*, 2003, **104**, 635–638.
- 23 A. Bergamo, M. Cocchietto, I. Capozzi, G. Mestroni, E. Alessio and G. Sava, *Anti-Cancer Drugs*, 1996, **7**, 697.
- 24 A. Bergamo, S. Zorzet, B. Gava, A. Sorc, E. Alessio, E. Iengo and G. Sava, *Anti-Cancer Drugs*, 2000, **11**, 665–672.
- 25 A. Bergamo, S. Zorzet, M. Cocchietto, M. E. Carotenuto, M. Magnarin and G. Sava, *Anticancer Res.*, 2001, **21**, 1893–1898.
- 26 M. Pongratz, P. Schluga, M. A. Jakupec, V. B. Arion, C. G. Hartinger, G. N. Allmaier and B. K. Keppler, *J. Anal. At. Spectrom.*, 2004, **19**, 46–51.
- 27 A. Bergamo, L. Messori, F. Piccioli, M. Cocchietto and G. Sava, *Invest. New Drugs*, 2003, **21**, 401–411.
- 28 A. Bergamo and G. Sava, *Dalton Trans.*, 2007, 1267–1272.
- 29 M. Liu, Z. Lim, Y. Gwee, A. Levina and P. Lay, *Angew. Chem., Int. Ed.*, 2010, **49**, 1661–1664.
- 30 C. M. Weekley, J. B. Aitken, S. Vogt, L. A. Finney, D. J. Paterson, M. D. de Jonge, D. L. Howard, P. K. Witting, I. F. Musgrave and H. H. Harris, *J. Am. Chem. Soc.*, 2011, **133**, 18272–18279.
- 31 T. Paunesku, S. Vogt, J. Maser, B. Lai and G. Woloschak, *J. Cell. Biochem.*, 2006, **99**, 1489–1502.
- 32 E. Crossley, J. Aitken, S. Vogt, H. Harris and L. Rendina, *Angew. Chem., Int. Ed.*, 2010, **49**, 1231–1233.
- 33 J. B. Aitken, E. A. Carter, H. Eastgate, M. J. Hackett, H. H. Harris, A. Levina, Y.-C. Lee, C.-I. Chen, B. Lai, S. Vogt and P. A. Lay, *Radiat. Phys. Chem.*, 2010, **79**, 176–184.
- 34 A. Levina, H. H. Harris and P. A. Lay, *J. Am. Chem. Soc.*, 2007, **129**, 1065–1075.
- 35 K.-G. Lipponer, E. Vogel and B. K. Keppler, *Met.-Based Drugs*, 1996, **3**, 243–260.
- 36 M. A. Jakupec, M. Galanski, V. B. Arion, C. G. Hartinger and B. K. Keppler, *Dalton Trans.*, 2008, 183–194.
- 37 G. Mestroni, E. Alessio and G. Sava, *WO Patent*, WO/1998/000,4311998.
- 38 E. A. Carter, B. S. Rayner, A. I. Mcleod, L. E. Wu, C. P. Marshall, A. Levina, J. B. Aitken, P. K. Witting, B. Lai, Z. Cai, S. Vogt, Y.-C. Lee, C.-I. Chen, M. J. Tobin, H. H. Harris and P. A. Lay, *Mol. BioSyst.*, 2010, **6**, 1316–1322.
- 39 C. M. Weekley, J. B. Aitken, S. Vogt, L. A. Finney, D. J. Paterson, M. D. de Jonge, D. L. Howard, I. F. Musgrave and H. H. Harris, *Biochemistry*, 2011, **50**, 1641–1650.
- 40 J. B. Waern, H. H. Harris, B. Lai, Z. Cai, M. M. Harding and C. T. Dillon, *JBIC, J. Biol. Inorg. Chem.*, 2005, **10**, 443–452.
- 41 M. Hannon, *Pure Appl. Chem.*, 2007, **79**, 2243–2261.
- 42 F. Frausin, M. Cocchietto, A. Bergamo, V. Searcia, A. Furlani and G. Sava, *Cancer Chemother. Pharmacol.*, 2002, **50**, 405–411.